Magnesium hydrazinidoborane: Synthesis, characterization and features for solid-state hydrogen storage

Carlos Castilla-Martinez, Lucas Roussignol, Umit Demirci

Version of Record: https://www.sciencedirect.com/science/article/pii/S0360319921028676
Manuscript_f10d3730567cc69d128c6088ed4f451b

Magnesium hydrazinidoborane: Synthesis, characterization and features for solid-state hydrogen storage

Carlos A. CASTILLA-MARTINEZ,* Lucas ROUSSIGNOL, Umit B. DEMIRCI*

Institut Européen des Membranes, IEM – UMR 5635, Univ Montpellier, ENSCM, CNRS, Montpellier, France
**Corresponding authors:* ccastilla90@gmail.com; umit.demirci@umontpellier.fr

Abstract

After various attempts, we present a new alkaline-earth derivative of hydrazine borane ($N_2H_4BH_3$, HB), magnesium hydrazinidoborane ($Mg(N_2H_3BH_3)_2$, $Mg(HB)_2$, 10.5 wt. % H), that was undoubtedly identified by FTIR and ^{11}B MAS NMR spectroscopy. $Mg(HB)_2$ was obtained by an alternative synthesis route, which is the reaction between HB and di-n-butylmagnesium in THF. The dehydrogenation properties of this compound were evaluated by two different approaches: an "open" system by thermogravimetric analysis and differential scanning calorimetry, and in a closed system, by heating the compound under isothermal conditions. Different results were obtained depending on the approach. Unlike other boron- and nitrogen-based compounds, it is likely that when $Mg(HB)_2$ is heated in a closed system, the dehydrogenation is limited and it occurs mainly due to the homopolar interaction between the protic hydrogen atoms of the molecule. Also, $Mg(HB)_2$ presents a contrasting thermal behavior in comparison with previous HB derivatives. In addition, a characterization by X-ray photoelectron spectroscopy was performed, and we detected instability of $Mg(HB)_2$ when it was irradiated with the X-ray beam. All of these results are presented and discussed in the context of materials for hydrogen storage in the solid-state.

Keywords

Hydrazine borane; Hydrazinidoborane; Hydrogen storage; Magnesium.

1. Introduction

Nowadays, fossil fuels are the main source of energy for humanity. Every year, the energy demand increases and consequently, fossil fuels are being depleted. Furthermore, the burning of these fuels is the main contributor of the release of greenhouse gases into the atmosphere and thus, of global warming. With this background, the need of a cleaner and an abundant source of energy is imperative. The best substitute for fossil fuels appears to be hydrogen [1,2]. The reasons to consider hydrogen as the fuel of the future are diverse: it has the highest energy content of any known fuel, it is non-toxic, it is abundant as an element, it can be produced from clean sources, it produces zero pollutant emissions and it can be used in both stationary and mobile applications [3,4]. However, the infrastructure for a future based on hydrogen still requires of much effort to be done. In this context, one of the main challenges of hydrogen technologies is hydrogen storage.

Hydrogen can be stored in high pressure vessels, at low temperature or in a material [5]. The latest technology is the most promising and different approaches have been investigated to obtain materials with a high hydrogen storage capacity. Hydrogen can be stored through electrochemical methods [6]. Hydrogen is also stored via physical or chemical interactions within a material. Different types of materials have been considered depending on the type of interaction. For example, for hydrogen physisorption, carbon materials, zeolites and metal organic frameworks have been envisaged; meanwhile for hydrogen chemisorption, compounds like liquid ammonia, boron and nitrogen-based materials or complex/intermetallic hydrides have been considered [7–10].

Boron and nitrogen-based materials have been intensely studied for chemical hydrogen storage [11–13]. These compounds have advantageous characteristics: (i) B and N are light atoms that can bind with multiple hydrogen atoms, giving a high H_2 content to these compounds; (ii) characteristic heteropolar dihydrogen interactions [14], which allows the molecules to release H_2 at mild conditions ; and (iii) these compounds are solid at ambient conditions and stable under an inert atmosphere.

One of the most representative example of boron- and nitrogen-based compounds is ammonia borane (NH_3BH_3, AB) [15]. AB is a widely studied material that carries 19.5 wt. % H and it has

been considered for solid-state hydrogen storage. Despite the high hydrogen content of the material, the release of H_2 starts at high temperature (at about 100 °C) and during thermolysis, undesired byproducts like ammonia NH_3 and borazine $B_3N_3H_6$ are produced. Another representative boron- and nitrogen-based compound is a derivative of AB, hydrazine borane ($N_2H_4BH_3$, HB, 15.4 wt. % H) [16–18]. Compared to AB, HB starts to dehydrogenate at a lower temperature, at about 60 °C. However, HB also suffers the formation of undesired byproducts (N_2H_4 and NH_3). In addition, it forms a shock-sensitive product when heated above 300 °C. Like in the case of AB, the use of pristine HB for hydrogen storage in the solid state is not viable.

Different approaches have been proposed in order to overcome the issues encountered by HB. The chemical modification of HB, substituting one of the $H^{\delta+}$ of the hydrazine moiety of the molecule by an alkali metal cation M^+ is one of those options. These compounds are called alkali hydrazinidoboranes (denoted MHB). Up to now, all the alkali hydrazinidoboranes have been synthesized: LiHB ($LiN_2H_3BH_3$, 11.7 wt. % H), NaHB ($NaN_2H_3BH_3$, 8.9 wt. % H), KHB ($KN_2H_3BH_3$, 7.2 wt. % H), RbHB ($RbN_2H_3BH_3$, 4.6 wt. % H) and CsHB ($CsN_2H_3BH_3$, 3.4 wt. % H) [19–24]. The synthesis reactions of alkali hydrazinidoboranes were carried out between HB and the respective alkali metal hydride or pure metal, following the subsequent reactions:

$$MH + NH_2NH_2BH_3 \rightarrow NH_2NH(M)BH_3 + H_2 \quad (1)$$

$$M + NH_2NH_2BH_3 \rightarrow NH_2NH(M)BH_3 + ½\ H_2 \quad (2)$$

With M = Li, Na, K for (1) and M = Rb, Cs for (2). All of these compounds are crystalline at ambient conditions, and they have shown better dehydrogenation properties than HB. The introduction of the metal cation in the molecule causes the destabilization of the molecule and all alkali hydrazinidoboranes start to dehydrogenate at a lower temperature than HB. Unfortunately, all of them release undesired byproducts. Besides, the solid residues after dehydrogenation have shown a complex composition and the identification of such chemical species is still a big challenge, and makes the regeneration of the material difficult.

Further research has been done in order to investigate the destabilization effect of alkaline earth atoms on HB, to obtain the alkaline earth hydrazinidoboranes ($M(N_2H_3BH_3)_2$, $M(HB)_2$). Up to now, the only example is the calcium derivative $Ca(HB)_2$ ($Ca(N_2H_3BH_3)_2$, 9.3 wt. % H) [25]. However, $Ca(HB)_2$ could not be obtained as a pure phase: the material is a mixture of the

precursor CaH_2, and the new phase $Ca(HB)_2$. Furthermore, the synthesis conditions are very particular: the mixture CaH_2:2HB has to be ball milled, heated at 1 °C min^{-1} up to 62 °C, kept at that temperature for 50 min and then quickly cooled down to room temperature. Despite all the effort to obtain the compound, it dehydrogenates in the range 90-170 °C and releases undesired byproducts (NH_3, N_2H_4 and N_2).

In the past, our research group has tried to synthesize the magnesium derivative, $Mg(HB)_2$, in multiple ways, but all of them had failed [26,27]. In this study, we finally obtained $Mg(HB)_2$, through a wet method that we developed accordingly. This method has not been previously used for the synthesis of hydrazinidoboranes, and it consists in the direct reaction between HB and a metal alkyl precursor, di-n-butylmagnesium, in THF. $Mg(HB)_2$ carries 10.6 wt. % H, which represents more H than any of the alkali hydrazinidoboranes (with the exception of LiHB). The thermal properties of the magnesium derivative are in contrast with previous hydrazinidoboranes. The characterization and evaluation of the dehydrogenation properties of $Mg(HB)_2$, were carried out in this study and are presented hereafter.

2. Materials and methods

2.1 Reagents

Commercial hydrazine hemisulphate (N_2H_4•½H_2SO_4, Sigma-Aldrich, ≥98 %), sodium borohydride ($NaBH_4$, Sigma-Aldrich, ≥98 %) and 1,4-dioxane (Sigma-Aldrich, anhydrous, ≥99.8%) were used to synthesize HB. Di-n-butylmagnesium solution (Sigma-Aldrich, 1.0 M in heptane) was used as the source of magnesium, and THF (Acros Organics, extra dry, 99.5 %) was used as the solvent in the synthesis of $Mg(HB)_2$.

2.2 Synthesis

2.2.1 Synthesis of HB

The experiments were carried out under an inert atmosphere using either a glove box (MBraun M200B; O_2< 0.1 ppm and H_2O< 0.1 ppm) or a Schlenk line. HB is synthesized by a method that was developed and optimized in our lab [28]. In this synthesis route, 21.59 g of N_2H_4·½H_2SO_4 and 10.12 g of $NaBH_4$ are weighed in the glove box and put in a flask, which is transferred

outside the glove box. Once connected to the Schlenk line, both reactants are suspended in 150 mL of 1,4-dioxane in a round-bottom Schlenk under stirring at 30 °C for 48 h. The obtained suspension is filtered and then, the solvent of the obtained solution is removed under vacuum. With this route, almost pure HB is obtained (>99.5 % pure, with a yield of approximately 80 %). The synthesis reaction is written as follows:

$$NaBH_4 + N_2H_4 \cdot \frac{1}{2}H_2SO_4 \rightarrow N_2H_4BH_3 + \frac{1}{2}Na_2SO_4 + H_2 \quad (3)$$

2.2.2 Synthesis of $Mg(HB)_2$

Inside the glovebox, 0.300 g of HB were dissolved in 20 mL of anhydrous THF under stirring. With a syringe, 3 mL of the di-n-butylmagnesium were added dropwise. The molar ratio HB:Mg was of 2:1, with a 10% excess of HB. After the first drops were added, a white precipitate formed, and the release of gaseous butane was observed (Supplementary Material (SM), Figure S1). The suspension was maintained under stirring for 20 h. The overall reaction can be written as follows:

$$2N_2H_4BH_3 + [CH_3(CH_2)_3]_2Mg \rightarrow Mg(N_2H_3BH_3)_2 + 2C_4H_{10} \quad (4)$$

After this time, the white suspension was centrifuged for 15 min at 5500 rpm. The solvent was removed and fresh THF was added to wash the product and remove any remaining HB. This process was repeated twice. The washed product was collected into a vial and it was introduced into a round bottom Schlenk flask. Right after, the flask was taken out of the glovebox and it was connected to the Schlenk line to be dried under vacuum overnight (at room temperature). Finally, the product, in the form of a white powder, was recovered and stored inside the glovebox for further analyses.

2.3 Characterization

2.3.1 Structural characterization

$Mg(HB)_2$ and the dehydrogenated solid residues were analyzed by Fourier Transformed Infrared spectroscopy (FTIR, NEXUS instrument, ThermoFisher Scientific, equipped with an attenuated total reflection accessory from 600 to 4000 cm^{-1} wavenumber, 32 scans). The samples were prepared inside the glove box in vials, and analyzed under air, taking them out of the vial at the last moment before the analysis. The same samples were also analyzed by solid-state ^{11}B magic

angle spinning nuclear magnetic resonance (MAS NMR; Varian VNMR4000, 128.31 MHz). ZrO_2 rotors of 3.2 mm in diameter were used for the analyses.

Powder X-ray diffraction (PXRD) was used to characterize all the samples. A PANalytical X'pert Pro diffractometer in Bragg-Brentano geometry was used. The samples were analyzed over the 2θ range of 10-65°. All the samples were prepared inside the glovebox, and they were protected from air by a Kapton film. X-ray Photoelectron Spectroscopy (XPS) analyses were performed with a spectrometer Escalab 250Xi (ThermoElectron), equipped with an Al-K_α monochromatized source (1486.6 eV). The binding energy was calibrated with the C 1s reference at 285.0 eV. In addition, some liquid-state Nuclear Magnetic Resonance analyses were performed (NMR; Bruker Avance; 9 T; 400 MHz, CD_3CN as deuterated solvent).

2.3.2 Thermal characterization

$Mg(HB)_2$ was analyzed using simultaneous thermogravimetric (TG) and differential scanning calorimetry (DSC) analyses, in an SDT Q600 apparatus (TA Instruments). In addition, a TG analysis (Netzsch STA 449 F1 Jupiter) coupled with a mass spectrometer (MS; Netzsch QMS 403 D Aëolos Quadro) was performed to analyze the evolved gases from the sample. The samples were prepared inside the glove box, where the powder was enclosed in an aluminum Tzero hermetic pan to keep it under inert atmosphere. Before the analysis, the pan was pierced with a needle to allow the gases to escape.

The decomposition behavior of $Mg(HB)_2$ was analyzed at isothermal condition at different temperatures (80, 100 and 120 °C) in a stainless-steel reactor. In the glove box, 80 mg of the sample was weighed and placed in a glass vial inside the reactor. The reactor was transferred outside the glove box, connected to a pressure controller and immersed in an oil bath at the required temperature. The change of pressure was monitored as a function of time. The equivalents of gas liberated were calculated considering the gas as ideal. The time period in which the reactor passes from room temperature to the analysis temperature was not considered.

The gases released by the sample were analyzed with a gas chromatograph (GC; PerkinElmer Clarus 400 equipped with a ShinCarbon ST 100/120 Restek column), using helium as the vector gas. The GC is coupled with a mass spectrometer (MS; PerkinElmer Clarus 600 T, equipped

with an Elite-GC Molesieve and an Elite Plot Q column). Typically, a sample of 100 µL of gas was taken with a glass syringe and injected into the GC-MS.

3. Results and discussion

3.1 Preliminary comments

$Mg(HB)_2$ is a white powder at room temperature. Tests of solubility in anhydrous organic solvents were unsuccessful for THF, 1-4 dioxane, toluene and dimethyl carbonate. Regarding protic solvents, $Mg(HB)_2$ violently reacts with water (hydrolysis reaction), with a fast H_2 release. The same happens, at a slower rate, for methanol, ethanol and isopropanol (alcoholysis reactions). This behavior is typical of the alkali hydrazinidoboranes and of AB derivatives (amidoboranes) [19,21,23,29]. When $Mg(HB)_2$ was treated at 400 °C, the solid product recovered was stable; in comparison with HB, the generation of a shock-sensitive product was avoided. Ion conductivity experiments were carried out to test the effect of the Mg^{2+} in the material. Nevertheless, the sample was not at all conductive.

3.2 Molecular structure of $Mg(HB)_2$

$Mg(HB)_2$ was analyzed by FTIR and the spectrum was compared with that of HB (Figure 1). As it can be observed, $Mg(HB)_2$ presents all the characteristic bands of B- and N-based compounds, and the spectrum is similar to those of the other hydrazinidoboranes [20,21,23,24]. The N–H stretching bands can be seen in the range 2800-3400 cm^{-1}, while the B–H stretching vibration modes are observed between 2000-2600 cm^{-1}. However, the spectrum is different from that of the parent HB [28]. Both the N–H and B–H vibrational modes are less complex in $Mg(HB)_2$ in comparison with HB. This indicates a difference in the bonding and electronic structure in the $N_2H_4^-$ of HB and the Mg–$N_2H_3^-$ of $Mg(HB)_2$, and this is due to weaker interactions between the protic $H^{\delta+}$ and the hydridic $H^{\delta-}$ hydrogens in the molecule [30]. The same trend can be seen in the N–H bending region (1300-1600 cm^{-1}). In addition, in the case of HB, the B–N bond appears at 749 cm^{-1} and for $Mg(HB)_2$, it has blue-shifted to 790 cm^{-1}, indicating an increase in energy, and thus a shortening of the B–N bond, characteristic of hydrazinidoboranes [31].

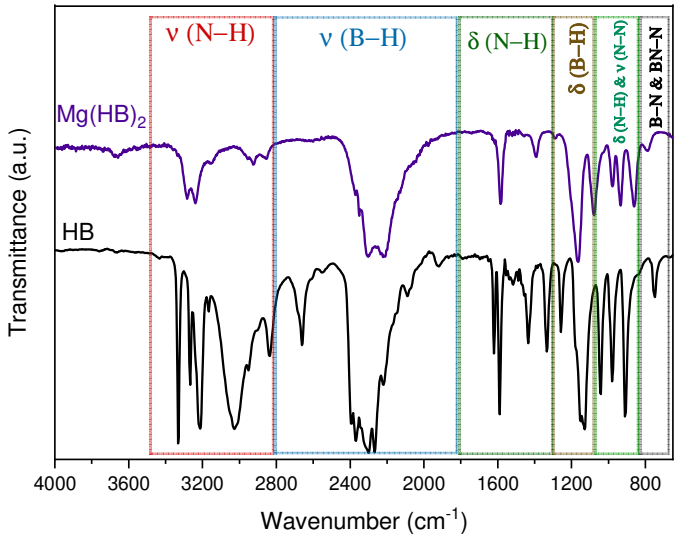

Figure 1. FTIR spectra of HB and $Mg(HB)_2$. The bands have been assigned.

$Mg(HB)_2$ was analyzed by ^{11}B MAS NMR spectroscopy and its spectrum was compared with that of HB (Figure 2). HB presents a single signal with a split shape centered at -24 ppm, indicating an NBH_3 environment. This shape is characteristic of a quadrupolar effect of the boron, indicating anisotropy around the atom [32–34]. In the case of $Mg(HB)_2$, a single peak is observed at -19 ppm, corresponding to an NBH_3 environment. This symmetric signal indicates a change in the electronic environment around the boron atom, indicating a change from an anisotropic environment to an isotropic environment around it. The shift of this signal to a lower field and the symmetric shape are indubitable proof of the substitution of one of the protic hydrogens of the hydrazine moiety by the alkaline-earth cation, as this has been systematically observed for all alkali hydrazinidoboranes [20–24]. This shift indicates an increase in the electronic density around the N atom and thus, the shortening of the B–N bond, in agreement with the FTIR analysis. Another signal can be observed in the spectrum of $Mg(HB)_2$, centered at -8 ppm (marked with a star). We associate this signal with a slight decomposition of the material due to the MAS NMR analysis (due to the rotor rotation). This is a phenomenon that we have observed systematically during the MAS NMR analysis of several boron- and nitrogen-based compounds. However, we do not discard the possibility of a slight decomposition of the sample during the synthesis of the compound, due to the exothermicity of the reaction.

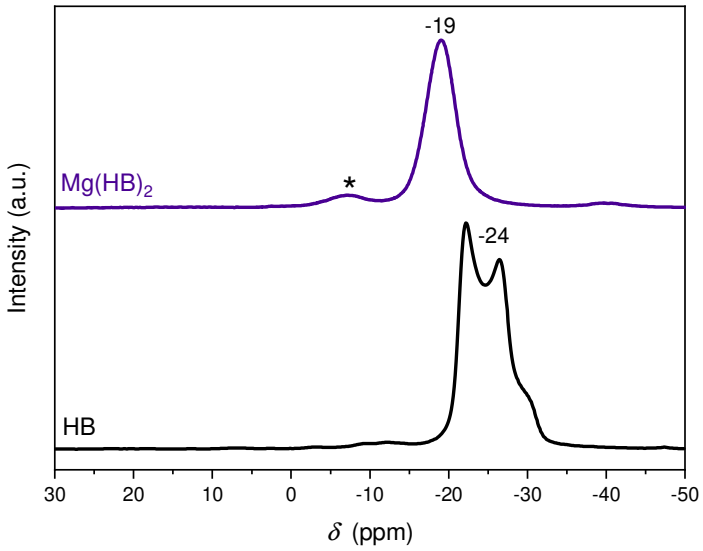

Figure 2. ^{11}B MAS NMR spectra of HB and $Mg(HB)_2$. The chemical shifts in ppm are indicated. The * indicates some byproducts due to a slight decomposition of the sample during the analysis.

$Mg(HB)_2$ was analyzed by PXRD (SM, Figure S2). No peaks can be found in the diffraction pattern. This indicates an amorphous compound. It is important to remark that the synthesis was tried out at low temperature (-5 °C), trying to slow down the kinetics of formation of $Mg(HB)_2$, but in all cases the results were the same.

3.3 Thermal decomposition of $Mg(HB)_2$

The thermal decomposition of $Mg(HB)_2$ was investigated by thermal gravimetric analysis and differential scanning calorimetry, with a heating ramp of 5 °C min^{-1}. The gases released by the sample were analyzed by MS. As shown in Figure 3, the compound starts to decompose at 60 °C and it loses 6 wt. % of the initial mass in the range of 60-115 °C. After this first loss, the material presents relative stability between 115 and 180 °C. In the range of 180-400 °C, the mass loss is of 11 wt. %. According to the MS results, the first loss of mass is mainly due to the release of N_2 and H_2. However, a small signal for m/z = 32 is also present, which indicates the evolution of N_2H_4. The second mass loss is related to the emission of N_2, H_2 and NH_3. The overall mass loss in the range of 40-400 °C is of 16.6 wt. %, which surpasses the hydrogen content of $Mg(HB)_2$,

that is of 10.5 wt. % H. If we consider a total dehydrogenation of the sample, this means that 6.1 wt. % of the mass loss is due to the emission of N_2, NH_3 and N_2H_4. At these conditions, no other volatile compounds were detected (i.e. B_2H_6 or $B_3N_3H_6$). A similar behavior was reported for calcium hydrazinidoborane [25].

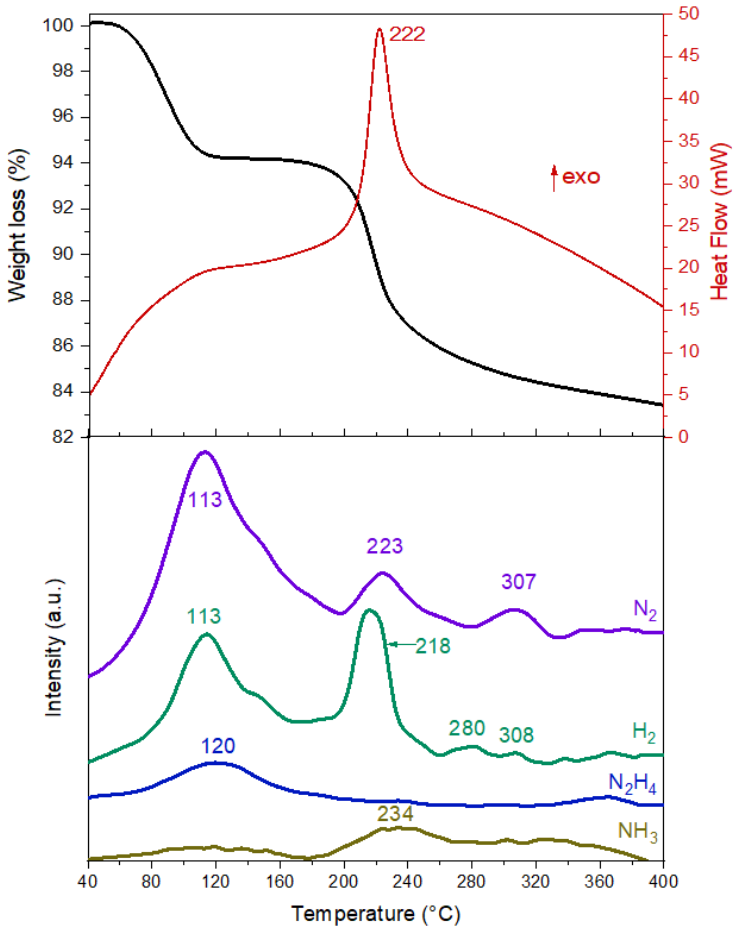

Figure 3. TGA-MS and DSC curves of $Mg(HB)_2$ (heating ramp of 5 °C min^{-1}). m/z = 2, 17, 28 and 32 for H_2, NH_3, N_2, and N_2H_4 respectively. The temperature in °C is indicated.

The DSC curve shows a single exothermic event at 222 °C. According to the MS analysis, there is an important release of H_2 and N_2 at 217 and 224 °C, respectively. The exothermic peak at 222 °C seems to be related to the emission of these two gases. In contrast with the alkali hydrazinidoboranes, $Mg(HB)_2$ does not show an endothermic process, and thus, it apparently does not melt. A similar behavior was found for $Ca(HB)_2$ [25].

The lack of theoretical calculations in the decomposition mechanisms of hydrazinidoboranes prevents us from giving an exact reaction pathway. However, we can propose a mechanism based on the available information. The evolution of N_2H_4, NH_3 and H_2 could be explained by the formation of an analogous compound of diammoniate of diborane ($[(NH_3)_2BH_2]^+[BH_4]^-$, DADB), a compound detected in the thermolysis of AB [35–39]. It is likely that the dehydrogenation of $Mg(HB)_2$ happens via the "metal cation driven hydride-transfer" mechanism (Figure 4) [40–42]. This mechanism implies the migration of a hydridic $H^{\delta-}$ hydrogen atom from the BH_3 moiety of the molecule to form a metal hydride intermediate with the metal cation (Mg–H). Just after, the $H^{\delta-}$ is transferred to the other $[N_2H_3BH_3]^-$ anion. This leads to the formation of an intermediate such as $[Mg(N_2H_3)_2BH_2]^+[BH_4]^-$. The dehydrocoupling reaction might continue due to this hypothetical species. Also, it is probable that parallel reactions might happen: due to the higher concentration of N_2H_3 with respect to the BH_2 groups, the formation of volatile products such as N_2 and NH_3 takes place, following equations (5) and (6).

$$2N_2H_3 \rightarrow 2NH_3 + N_2 \quad (5)$$

$$2N_2H_3 \rightarrow N_2H_4 + H_2 + N_2 \quad (6)$$

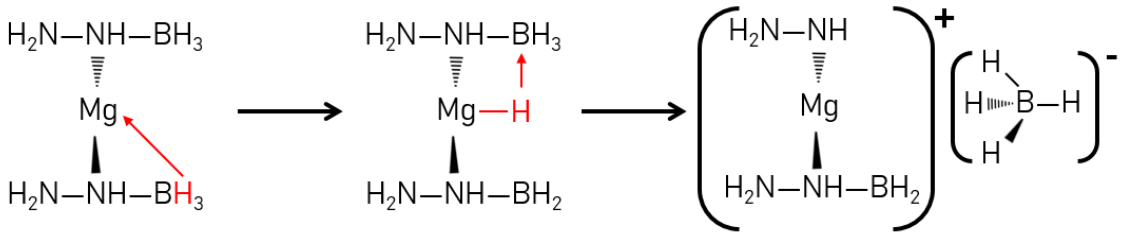

Figure 4. Proposed Mg^{2+} driven hydride-transfer mechanism of the possible formation of $[Mg(N_2H_3)_2BH_2]^+[BH_4]^-$ as reaction intermediate

According to the TGA curve, $Mg(HB)_2$ has a mass loss of about 6 wt. % up to 115 °C, and then it is thermally stable between 115-180 °C; after, it continues to decompose. Based on this, $Mg(HB)_2$ was analyzed after decomposition at 140 and 400 °C. Typically, 200 mg of $Mg(HB)_2$

were weighed and put in a stainless-steel reactor inside the glovebox. The reactor was transferred out of the glovebox and heated in a controlled furnace. The heating ramp was of 5 °C min^{-1} up to 140 °C, in order to maintain the conditions used in the TG analysis. The reactor was left for 5 min after the furnace reached 140 °C, and after this, it was taken out of the furnace and left to cool down to room temperature. To treat the sample at 400 °C, a tubular furnace was used. A flow of nitrogen (100 mL min^{-1}) was set and the sample was heated from room temperature to 400 °C with a ramp of 5 °C min^{-1}. After this, the sample was left to cool down in the furnace to room temperature. Both solid products were characterized.

The FTIR spectra of the samples heated at 140 and 400 °C, hereafter referred as MgHB140 and MgHB400 respectively, were compared with the one of $Mg(HB)_2$ (SM, Figure S3). Regarding MgHB140, a slight change can be seen in the N–H stretching band at about 2800 cm^{-1} that is less intense. However, no other visible changes are observed: the two spectra are practically identical. In the case of MgHB400, the N–H and B–H stretching bands have disappeared. Broad bands can be seen at about 760 cm^{-1} and at 1400 cm^{-1}, which belong to B–N vibrational modes.

The results of the ^{11}B MAS NMR analysis are shown in Figure 5. There are no changes between the fresh sample and the one heated with a ramp at 140 °C; the only signal is still present at -19 ppm, belonging to the NBH_3 environment. In the case of MgHB400, a broad signal can be seen in the positive chemical shifts. The signals that appear between 0-5 ppm belong to BN_4 environments [37,43]. The signals between 10-30 ppm are typical to trivalent boron species, and they are usually assigned to boron and nitrogen-based polymeric species, such as polyborazylene and/or boron nitride with BN_2H or BN_3 environments [44–46]. Also, it is possible that homopolar dehydrocoupling between the B atoms may occur, giving rise to B_2NH environments [47]. These signals are typically detected in the solid products after thermolysis of boron- and nitrogen-based compounds.

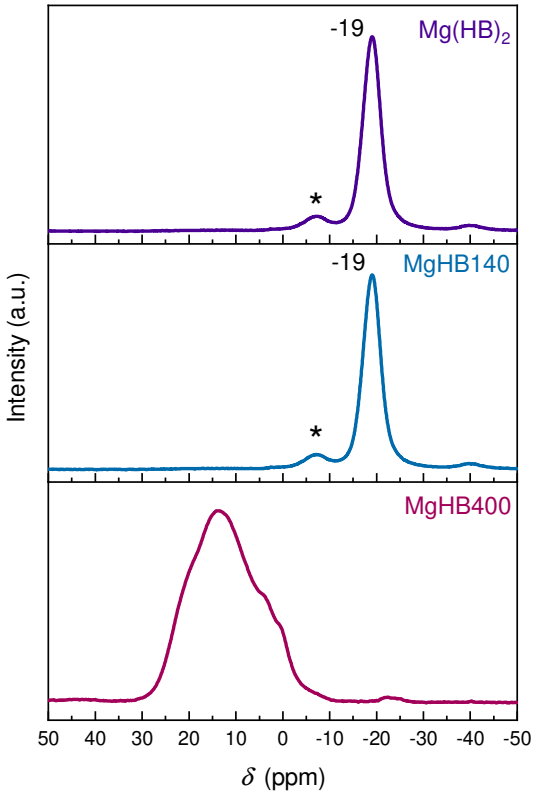

Figure 5. ^{11}B MAS NMR spectra of $Mg(HB)_2$, MgHB140 and MgHB400. The chemical shifts in ppm are indicated.

The PXRD patterns of the samples are shown in Figure 6. Broad peaks can be observed between 12-25°, indicated by the symbol #, which corresponds to the Kapton film used to protect the sample from air. For MgHB140, a single peak appeared at 18.2° when the sample was heated up to 140 °C. This peak does not correspond with any of the diffraction peaks of a possible compound formed during thermolysis, such as MgH_2, Mg or $Mg(BH)_4$. It is possible that a crystalline intermediate has formed in such conditions. However, we repeated the experiments heating fresh $Mg(HB)_2$ up to 125 and 155 °C and no diffraction peaks were detected in the patterns. In the case of MgHB400, the sample is amorphous, with a small signal presented at 42.7°. In this case, this peak could belong to MgO [48–50], which corresponds to the (2 0 0) plane. It is possible that some air entered in contact with the sample when introducing it into the

tubular furnace, which would result in the formation of small quantities of $Mg(OH)_2$, that would dehydrate to MgO with thermal treatment [51]. In addition, a broad signal appeared centered at 26°, that is associated with the formation of amorphous boron nitride [52].

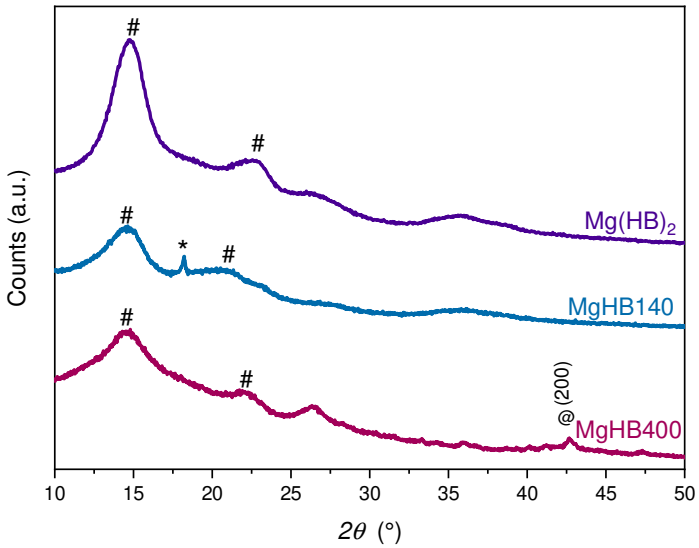

Figure 6. PXRD patterns of $Mg(HB)_2$, MgHB140 and MgHB400. The * indicates a diffraction peak of an unidentified compound. The @ indicates a diffraction peak that might belong to MgO. The # are bands assigned to the Kapton film used to protect the sample from air.

In order to have a better overview of the chemical state of $Mg(HB)_2$ and the solid products obtained after heat treatment at 140 and 400 °C, the samples were analyzed by XPS. The B 1s and N 1s spectra of the three samples are shown in Figure 7. For $Mg(HB)_2$, the B 1s spectrum shows two signals, one centered at 188.8 eV that is assigned to B–H bonds [53], and the other at 191.8 eV that can be assigned to a BN_xO_y species(B–O) [54–56]. This last signal is associated with a partial oxidation of the sample due to the exposure of the sample to the atmosphere. As the samples were packed and transported to perform the XPS analysis, it is probable that a small quantity of air could have entered the vial during transportation.

The N 1s spectrum of $Mg(HB)_2$ shows a single symmetrical signal centered at 400.9 eV, corresponding to a N_2–H_3 species [57]. After the sample is heated at 140 °C under argon

atmosphere, the intensity of the B–H signal decreases in the B 1s spectrum. The signal of the B–O species remains in the spectrum. In the case of the N 1s spectrum, the curve was deconvoluted into two signals, one centered at 400.7 eV which corresponds to the N_2–H_3 species, and a second one centered at 401.8 eV. This last signal is attributed to a N_2H_x ($1<x<3$) species [57]. This suggests a partial dehydrogenation of the N_2H_3 moiety of the molecule. At 400 °C, the B 1s spectrum presents the disappearance of the B–H signal and it shows a new signal at 190.5 eV, characteristic of B–N bonds in polyborazylene or boron nitride, in agreement with the ^{11}B MAS NMR analysis [55,56,58]. The N 1s spectrum of MgHB400 shows remaining species with N–H bonds, but the main new signal is centered at 398.1 eV, associated to the polyborazylene/boron nitride-like compounds.

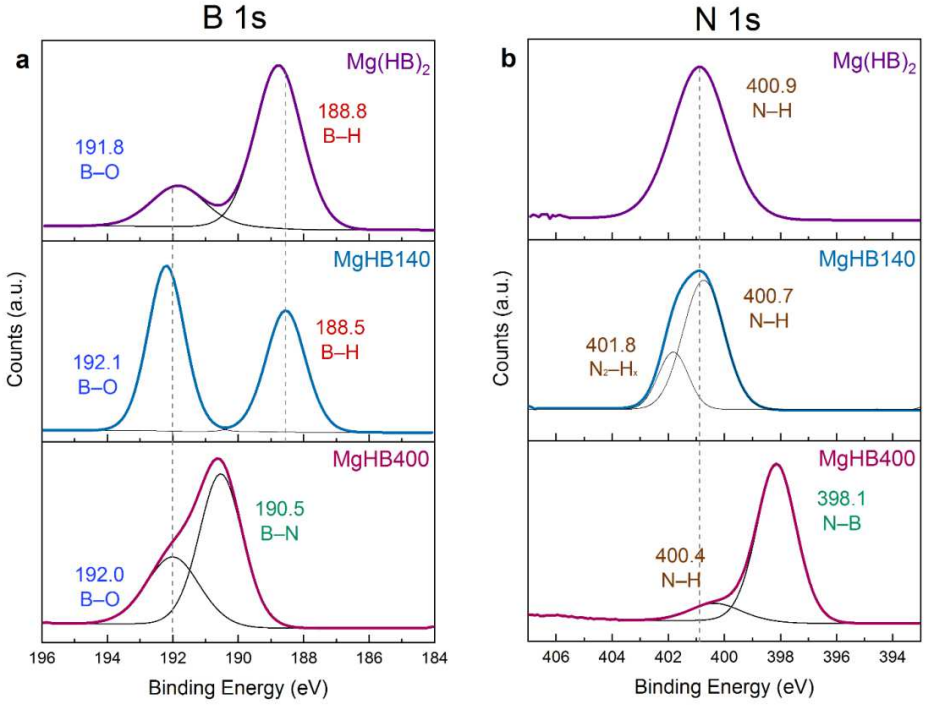

Figure 7. XPS spectra of $Mg(HB)_2$, MgHB140 and MgHB400 for a) B 1s and b) N 1s. The curves were deconvoluted with a Gaussian fit. The value of the binding energy in eV is indicated for each signal along with the associated species.

The spectra of Mg 2p and Mg KLL of $Mg(HB)_2$ for the samples MgHB140 and MgHB400 was obtained (SM. Figure S4). The Mg 2p spectra of all samples presents a symmetrical signal

centered at 50.0 ± 0.3 eV. As reported in the literature, the Mg KLL Auger signal of a Mg compound is composed of two main transitions, where the second peak has a higher intensity [59]. The kinetic energy reported for metallic Mg is 1185 eV, so in this case the Mg^{2+} state of the atom is confirmed, appearing at a lower value. The position of the Auger peaks at 1180 and 1175 eV suggest the formation of MgO [59–61]. However, the peak centered at 50.0 eV does not match with the expected value of MgO (at 51.0±0.2 eV) or of $Mg(OH)_2$ (49.3 eV) [62]. This might indicate a different bonding like Mg–N. Nevertheless, as the diffraction pattern presented in Figure 6 also suggested the formation of MgO, we do not discard the contribution of a small quantity of MgO or $Mg(OH)_2$ to these signals. The formation of these compounds might occur if the sample comes in contact with air at some point between the synthesis and the analyses (as previously explained, this might happen during transportation of the sample).

When the $Mg(HB)_2$ sample and the one heated at 140 °C were being analyzed by XPS, the evolution of the sample was observed due to the X-ray beam. We compared the spectra of the pristine samples with the spectra after some time under X-ray irradiation. As shown in Figure 8a, the B–H signal of $Mg(HB)_2$ decreased in intensity and broadened, indicating a dehydrogenation of the sample. This indicates an easy decomposition of the sample due to the exposure to the X-ray beam. In the case of MgHB140, the original signal merged in a single curve that was deconvoluted in three peaks. The apparition of the peak at 190.5 eV indicates the formation of B–N polymeric compounds, such as polyborazylene-like ones. The sample MgHB400 did not present any changes before and after the XPS analysis (not shown). It is evident that these samples decompose under the action of the X-ray beam. Based on these results, and in our experience with similar materials, we conclude that the analysis of borane compounds by XPS technique is hard, due to the prompt evolution (instability) of the samples under the X-ray beam. The B–O signal is still present and is centered at 191.5 eV. As previously mentioned, we associate this signal to the formation of BN_xO_y species due to the probable exposure of the sample to air during transportation.

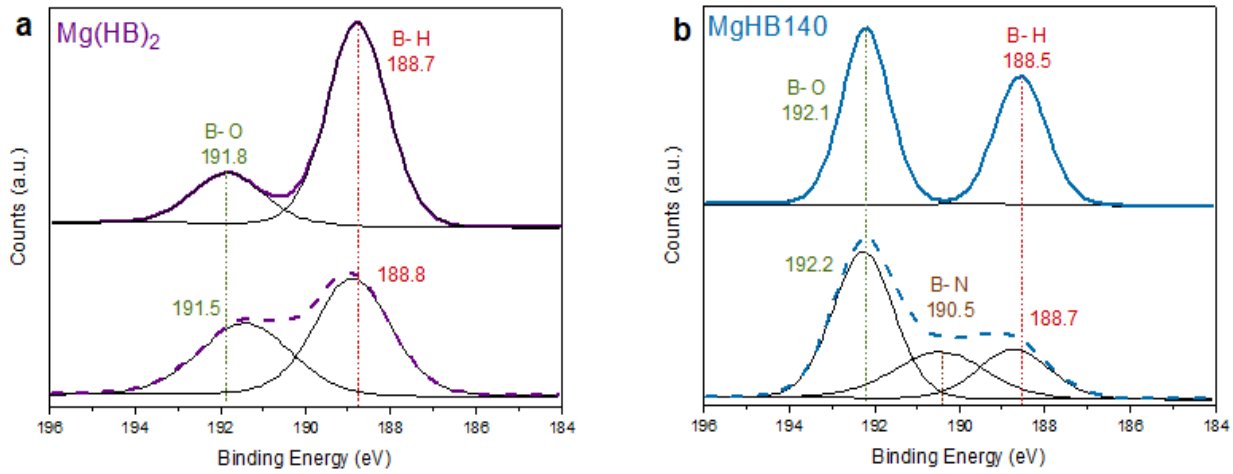

Figure 8. Evolution of the B 1s XPS spectra of a) $Mg(HB)_2$ and b) MgHB140. The spectra in dashed lines in the lower part of the graphics correspond to the evolved sample after some time under the X-ray beam. The spectra were deconvoluted with a Gaussian fit, and the binding energies (eV) and the assigned species are indicated on the figure.

3.4 Decomposition of $Mg(HB)_2$ under isothermal conditions

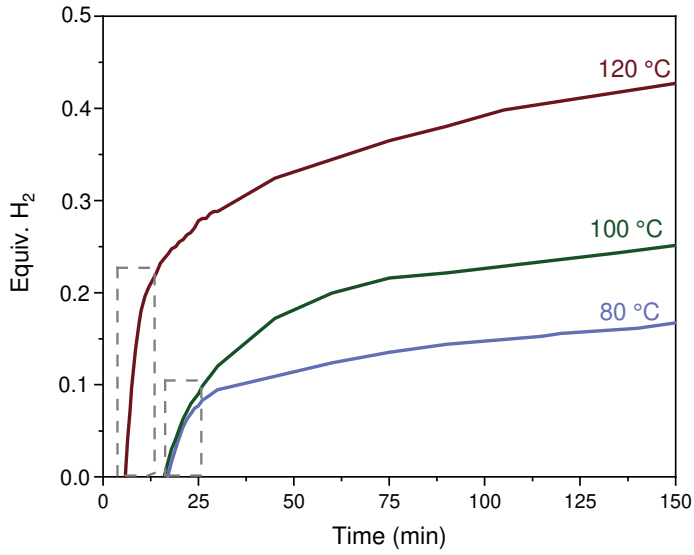

Figure 9. Time evolution of H_2 release from $Mg(HB)_2$ under heating at constant temperature (80, 100 and 120 °C). The initial faster release of H_2 is indicated by the dashed rectangles.

$Mg(HB)_2$ was heated under isothermal conditions at 80, 100 and 120 °C in order to evaluate the dehydrogenation rate of the compound. As shown in Figure 9, the decomposition of $Mg(HB)_2$ is a single step process. The three curves present the same behavior. The curves of 80 and 100 °C present an induction period of 18 min. After this, the sample starts to release H_2. A linear regression for the first steeper step of the dehydrogenation was performed (indicated by dashed rectangles in Figure 9) to calculate the initial rates of dehydrogenation. The dehydrogenation rates are 0.011, 0.013 and 0.037 equiv. H_2 min^{-1} for 80, 100 and 120 °C respectively. As expected, increasing the temperature increases the rate of generation of H_2. However, even at 120 °C, the equiv. H_2 released are not huge. After 120 min of heat treatment, the samples under isothermal conditions at 80, 100 and 120 °C release only 0.15, 0.23 and 0.40 equiv. H_2 respectively.

Regarding the dehydrogenation properties of $Mg(HB)_2$ at these conditions, the performance of $Mg(HB)_2$ is lower compared with other hydrazinidoboranes (SM, Figure S5) [21,23,28]. Even if we compare it with the parent HB at 100 °C, $Mg(HB)_2$ releases only a third of the quantity of gases released by HB after 1 h of heat treatment (0.2 vs. 0.65 respectively). This indicates that the introduction of the Mg^{2+} cation changed the behavior of HB, but it did not succeed in releasing more H_2 at lower temperatures. In other words, unlike any other HB derivative, $Mg(HB)_2$ is more thermally stable than HB.

The gases released by $Mg(HB)_2$ during the isothermal experiments at 80 and 100 °C were analyzed by GC-MS (SM, Figure S6 and Figure S7). In our conditions, the presence of H_2 is confirmed. As we cannot avoid the introduction of small quantities of air when injecting the sample, air was injected in the chromatogram as reference. The signals observed between 1 and 2 min belong to the retention time of N_2 and O_2 of air. The MS spectra for both samples show the presence of H_2, N_2 and O_2. It is difficult to affirm if the N_2 detected belongs only to the air, or if the gases released by the sample have a contribution to this signal. It is noticeable that under isothermal conditions and at 80 and 100 °C, no NH_3 and no N_2H_4 were detected.

The solid residues recovered after the isothermal experiments were analyzed by FTIR, PXRD and MAS NMR. The FTIR spectra of the solid residues show that, in concordance with the isothermal experiments, the dehydrogenation of the samples happened to a small extent (SM, Figure S8). The N–H and B–H stretching bands are still present in the spectra at 80, 100 and 120

°C. The PXRD analysis showed that there are no changes in the structure of the sample; all of them are amorphous (SM, Figure S9). The ^{11}B MAS NMR spectra of the solid residues were compared with that of $Mg(HB)_2$ (SM, Figure S10). In agreement with the FTIR and PXRD analyses, there are no visible changes in the spectra. The NBH_3 environment is the main signal for the solid residues treated at 80 and 100 °C. This indicates that the BH_3 moiety of $Mg(HB)_2$ is stable up to 120 °C, and that the H_2 generated might be mostly due to the N_2H_3 moiety.

Based on the previous results, it is likely that in a closed system and up to 140 °C, H_2 is released mainly by homopolar interactions ($H^{\delta+}\cdots H^{\delta+}$) of the N_2H_3 moiety, as the BH_3 environment remained unchanged. The species detected in the N 1s XPS spectrum of MgHB140 also supports this affirmation, where $Mg(HB)_2$ was heated in a closed stainless steel reactor. This is in contrast with ammonia borane and other boron- and nitrogen-based compounds, where the first dehydrogenation step typically involves both heteropolar and homopolar interactions [11,63]. It is the first time that we have detected this phenomenon in the dehydrogenation behavior of hydrazinidoboranes.

The low equiv. H_2 estimated by the isothermal experiments explains why all the spectra of the compound are pretty similar up to this temperature. However, under an "open" system (TGA), where the produced gases are being carried by the gas of the apparatus, a mass loss of 6 wt. % was detected. This is a phenomenon that has been frequently observed for amidoboranes/hydrazinidoboranes: the different thermal behavior of the compounds analyzed in a closed and an open system.

3.5 Stability of $Mg(HB)_2$

$Mg(HB)_2$ was stored under inert atmosphere and analyzed after 5 months of its synthesis by FTIR and ^{11}B MAS NMR (SM, Figure S11), and compared with the fresh sample. The spectra of both analyses show that there are no visible changes after the 5 months. $Mg(HB)_2$ is thus stable over long periods of time.

The behavior of $Mg(HB)_2$ was also analyzed under air atmosphere. A few milligrams were put in contact with air for 10 min and the powder was analyzed by FTIR. Surprisingly, the FTIR

spectrum of the sample resembled the HB spectrum. Further analyses were carried out in order to understand this behavior.

$Mg(HB)_2$ was exposed again to air for 10 min and immediately, it was put into an inert atmosphere. After, 1,4-dioxane was added to the sample. Part of the sample was solubilized and the other part precipitated. The suspension was centrifuged and separated. In the case of the part that was solubilized, the 1,4-dioxane was extracted and a white powder was obtained, and it was analyzed by FTIR and liquid ^1H NMR. The insoluble precipitate was dried under dynamic vacuum for 24 h and analyzed by FTIR.

The solid powder obtained after extraction of the solvent was identified as HB, based on the FTIR and the ^1H NMR spectra (SM, Figure S12). These results indicate that $Mg(HB)_2$ is sensitive to air and it can undergo a reversible reaction when it is taken out of an inert atmosphere, because it can react with the water present in the air. The following reaction is proposed:

$$Mg(N_2H_3BH_3)_2 + 2H_2O \rightarrow 2N_2H_4BH_3 + Mg(OH)_2 \quad (7)$$

Regarding the spectrum of the solid precipitate, it resembles that of $Mg(HB)_2$ (SM, Figure S13). However, a band appeared above 3600 cm^{-1} (O–H stretching). This can be explained by the formation of $Mg(OH)_2$. This also correlates with the detected signals in the XPS analysis (SM, Figure S4).

3.6 Hydrogen storage properties and perspectives

As previously mentioned, $Mg(HB)_2$, loses 6 % of weight between 60-120 °C, mainly due to the emission of N_2 and some H_2. A higher release of H_2 was detected with a sharper signal by the MS analysis at 218 °C. This is a different behavior than observed in previous alkali hydrazinidoboranes or other composites. For example, a mixture of MgH_2 and HB was prepared by ball milling and further analyzed [26]. Regarding the thermal behavior of the mixture, the mass loss is similar to that of HB. However, H_2 was released from 40 °C, showing a slight destabilization of HB due to the incorporation of MgH_2. In a similar way, some studies were performed in a mixture of MgH_2 and AB [64,65]. The destabilization of the mixture was demonstrated, where it released H_2 at lower temperatures in comparison with neat AB, and suppressed some of the gaseous byproducts.

We also compared the dehydrogenation behavior of $Mg(HB)_2$ with its analogous amidoborane. Magnesium amidoborane $Mg(AB)_2$ is a crystalline solid that releases about 10 wt. % H up to 300 °C [66]. However, in comparison with other amidoboranes, $Mg(AB)_2$ starts to release H_2 at a higher temperature (i.e. it is more stable). It seems that in order to release H_2, $Mg(AB)_2$ must overcome a large energetic barrier. The larger Pauling electronegativity of Mg, in comparison to other elements, is the origin of this barrier [67]. Interestingly, $Mg(HB)_2$ presents a similar higher thermal stability in comparison with the parent HB and other MHBs. This feature, together with the stability over time of this compound, might favor the potential use of this material for H_2 storage applications at temperatures such as 150-250 °C. Otherwise, $Mg(HB)_2$ might be considered as ceramic precursors. For example, it is known that AB and HB can be used as precursors of boron nitride (BN) [68,69]. The use of an alkali/alkaline earth hydrazinidoborane as precursor of BN might lead to the incorporation of the alkali or alkaline earth cation into the BN structure. Such functionalized BN structures have been proposed as potential materials for hydrogen storage [70,71].

We also have to mention another drawback about boron- and nitrogen-based materials for hydrogen storage applications: the regeneration of the dehydrogenated solid. As the dehydrogenation of these compounds is exothermic, the rehydrogenation is thermodynamically unfavorable. Different attempts have been proposed for the regeneration of AB [72–74], but implementing a cost-effective and efficient method has not been achieved yet. This is still a big challenge, if not the biggest, for boron- and nitrogen-based materials. A last issue is the purity of the H_2 released by these compounds. Many amidoboranes/hydrazinidoboranes release H_2 polluted with NH_3. The gas stream would require a purification system to deliver a highly pure H_2.

4. Conclusion

In this work, $Mg(HB)_2$ was obtained by an alternative synthesis route, which is the reaction between HB and n-dibutyl magnesium in THF. The new hydrazinidoborane was identified by different spectroscopy techniques. $Mg(HB)_2$ is a compound with a good stability over time and under inert atmosphere, but it showed a rapid evolution under the irradiation of a X-ray beam. Unlike any of the previous derivatives of HB, $Mg(HB)_2$ is thermally more stable than the parent

HB. Also, when $Mg(HB)_2$ is put into contact with air, the compound goes through a reversible process to form HB and $Mg(OH)_2$.

On the one hand, the thermal characterization under isothermal conditions showed that the dehydrogenation of $Mg(HB)_2$ is a one-step process (with an induction period of time), and it happens to a limited extent up to 120 °C, releasing only 0.40 equiv. H_2. Also under these conditions, the only byproduct detected was N_2. In contrast with other amidoboranes/hydrazinidoboranes, it appears that $Mg(HB)_2$ releases H_2 due to the homopolar interaction between N_2H_3 groups when the compound is heated in a closed system. On the other hand, the TGA-MS analysis showed the release of different byproducts along with H_2 (N_2, NH_3 and N_2H_4) and a considerable mass loss (16.6 wt. %) up to 400 °C. This indicates again the different thermal behavior of amidoboranes/hydrazinidoboranes depending on the conditions of the analysis (open/closed system).

Based on previous works, it is evident that the alkaline earth derivatives of HB are difficult to synthesize. Even if the magnesium derivative has a high content of H_2, it shows the production of undesired byproducts during their decomposition (N_2, NH_3, N_2H_4). This makes $Mg(HB)_2$, like the previously reported $Ca(HB)_2$, unsuitable for hydrogen storage at near-ambient conditions. Other prospects have been suggested, such as using $Mg(HB)_2$ as precursor of boron nitride-derived ceramics for H_2 storage, for example. It is likely that the Mg^{2+} in the molecule could have an impact on the properties of the ceramics after heat treatment.

5. Acknowledgments

The authors want to acknowledge the CONACyT (Mexican National Council for Science and Technology) for the scholarship of CACM. The authors acknowledge Sabine Devautour-Vinot (University of Montpellier) for the ion conductivity experiments performed for this work. A last acknowledgment for Christophe Charmette and Jim Cartier (University of Montpellier) for their valuable help with the GS-MS measurements.

References

[1] F. Dawood, M. Anda, G.M. Shafiullah, Hydrogen production for energy: An overview, Int. J. Hydrog. Energy, 45 (2020) 3847–3869.

[2] T. Van de Graaf, I. Overland, D. Scholten, K. Westphal, The new oil? The geopolitics and international governance of hydrogen, Energy Res. Soc. Sci., 70 (2020) 101667.

[3] B. Widera, Renewable hydrogen implementations for combined energy storage, transportation and stationary applications, Therm. Sci. Eng. Prog., 16 (2020) 100460.

[4] A. Pareek, R. Dom, J. Gupta, J. Chandran, V. Adepu, P.H. Borse, Insights into renewable hydrogen energy: Recent advances and prospects, Mater. Sci. Energy Technol., 3 (2020) 319–327.

[5] R. Moradi, K.M. Groth, Hydrogen storage and delivery: Review of the state of the art technologies and risk and reliability analysis, Int. J. Hydrog. Energy, 44 (2019) 12254–12269.

[6] M. Kaur, K. Pal, Review on hydrogen storage materials and methods from an electrochemical viewpoint, J. Energy Storage, 23 (2019) 234–249.

[7] A. El Kharbachi, E.M. Dematteis, K. Shinzato, S.C. Stevenson, L.J. Bannenberg, M. Heere, C. Zlotea, P. Szilágyi, J.P. Bonnet, W. Grochala, D.H. Gregory, T. Ichikawa, M. Baricco, B.C. Hauback, Metal hydrides and related materials. Energy carriers for novel hydrogen and electrochemical storage, J. Phys. Chem. C, 124 (2020) 7599–7607.

[8] M. Hirscher, V.A. Yartys, M. Baricco, J. Bellosta von Colbe, D. Blanchard, R.C. Bowman, D.P. Broom, C.E. Buckley, F. Chang, P. Chen, Y.W. Cho, J.C. Crivello, F. Cuevas, W.I.F. David, P.E. de Jongh, R. V. Denys, M. Dornheim, M. Felderhoff, Y. Filinchuk, G.E. Froudakis, et al., Materials for hydrogen-based energy storage – past, recent progress and future outlook, J. Alloys Compd., 827 (2020).

[9] Y. Kojima, Hydrogen storage materials for hydrogen and energy carriers, Int. J. Hydrog. Energy, 44 (2019) 18179–18192.

[10] Y. Luo, Q. Wang, J. Li, F. Xu, L. Sun, Y. Zou, H. Chu, B. Li, K. Zhang, Enhanced hydrogen storage/sensing of metal hydrides by nanomodification, Mater. Today Nano, 9

(2020).

[11] R. Kumar, A. Karkamkar, M. Bowden, T. Autrey, Solid-state hydrogen rich boron-nitrogen compounds for energy storage, Chem. Soc. Rev., 48 (2019) 5350–5380.

[12] K. Wang, Z. Pan, X. Yu, Metal B-N-H hydrogen-storage compound: Development and perspectives, J. Alloys Compd., 794 (2019) 303–324.

[13] Q. Yao, Y. DIng, Z.H. Lu, Noble-metal-free nanocatalysts for hydrogen generation from boron- and nitrogen-based hydrides, Inorg. Chem. Front., 7 (2020) 3837–3874.

[14] E. Magos-Palasyuk, A. Litwiniuk, T. Palasyuk, Experimental and theoretical evidence of dihydrogen bonds in lithium amidoborane, Sci. Rep., 10 (2020) 1–12.

[15] S. Akbayrak, S. Özkar, Ammonia borane as hydrogen storage materials, Int. J. Hydrog. Energy, 43 (2018) 18592–18606.

[16] T. Hu, M.F. Ku, D. Lentz, Hydrazine borane : A promising hydrogen storage material, J. Am. Chem. Soc., 131 (2009) 7444–7446.

[17] W. Wang, X. Hong, Q. Yao, Z.H. Lu, Bimetallic Ni-Pt nanoparticles immobilized on mesoporous N-doped carbon as a highly efficient catalyst for complete hydrogen evolution from hydrazine borane, J. Mater. Chem. A, 8 (2020) 13694–13701.

[18] Q. Yao, K. Yang, W. Nie, Y. Li, Z.H. Lu, Highly efficient hydrogen generation from hydrazine borane via a MoO_x-promoted NiPd nanocatalyst, Renew. Energy, 147 (2020) 2024–2031.

[19] H. Wu, W. Zhou, F.E. Pinkerton, T.J. Udovic, T. Yildirim, J.J. Rush, Metal hydrazinoborane $LiN_2H_3BH_3$ and $LiN_2H_3BH_3{\cdot}2N_2H_4BH_3$: crystal structures and high-extent dehydrogenation, Energy Environ. Sci., 5 (2012) 7531–7535.

[20] R. Moury, U.B. Demirci, V. Ban, Y. Filinchuk, T. Ichikawa, L. Zeng, K. Goshome, P. Miele, Lithium hydrazinidoborane: A polymorphic material with potential for chemical hydrogen storage, Chem. Mater., 26 (2014) 3249–3255.

[21] R. Moury, U.B. Demirci, T. Ichikawa, Y. Filinchuk, R. Chiriac, A. Van Der Lee, P. Miele, Sodium hydrazinidoborane: A chemical hydrogen-storage material, ChemSusChem, 6

(2013) 667–673.

[22] Y.S. Chua, Q. Pei, X. Ju, W. Zhou, T.J. Udovic, G. Wu, Z. Xiong, P. Chen, H. Wu, Alkali metal hydride modification on hydrazine borane for improved dehydrogenation, J. Phys. Chem. C, 118 (2014) 11244–11251.

[23] C.A. Castilla-Martinez, D. Granier, C. Charmette, G. Maurin, P.G. Yot, U.B. Demirci, Rubidium hydrazinidoborane: Synthesis, characterization and hydrogen release properties, Int. J. Hydrog. Energy, 44 (2019) 28252–28261.

[24] C.A. Castilla-Martinez, D. Granier, C. Charmette, J. Cartier, P.G. Yot, U.B. Demirci, Cesium hydrazinidoborane, the last of the alkali hydrazinidoboranes, studied as potential hydrogen storage material, Int. J. Hydrog. Energy, 45 (2020) 16634–16643.

[25] S. Ould-Amara, V. Yadav, E. Petit, G. Maurin, P.G. Yot, U.B. Demirci, Calcium hydrazinidoborane: Synthesis, characterization, and promises for hydrogen storage, Int. J. Hydrog. Energy, 45 (2019) 2022–2033.

[26] S. Pylypko, J.F. Petit, S. Ould-Amara, N. Hdhili, A. Taihei, R. Chiriac, T. Ichikawa, M. Cretin, P. Miele, U.B. Demirci, Metal hydride-hydrazine borane: Towards hydrazinidoboranes or composites as hydrogen carriers, Int. J. Hydrog. Energy, 40 (2015) 14875–14884.

[27] C.A. Castilla-Martinez, R. Moury, U.B. Demirci, Amidoboranes and hydrazinidoboranes: State of the art, potential for hydrogen storage, and other prospects, Int. J. Hydrog. Energy, 45 (2020) 30731–30755.

[28] R. Moury, G. Moussa, U.B. Demirci, J. Hannauer, S. Bernard, E. Petit, A. Van Der Lee, P. Miele, Hydrazine borane: Synthesis, characterization, and application prospects in chemical hydrogen storage, Phys. Chem. Chem. Phys., 14 (2012) 1768–1777.

[29] Y.S. Chua, P. Chen, G. Wu, Z. Xiong, Development of amidoboranes for hydrogen storage, Chem. Commun., 47 (2011) 5116–5129.

[30] D.Y. Kim, H.M. Lee, J. Seo, S.K. Shin, K.S. Kim, Rules and trends of metal cation driven hydride-transfer mechanisms in metal amidoboranes, Phys. Chem. Chem. Phys., 12 (2010) 5446–5453.

[31] Z. Xiong, C.K. Yong, G. Wu, P. Chen, W. Shaw, A. Karkamkar, T. Autrey, M.O. Jones, S.R. Johnson, P.P. Edwards, W.I.F. David, High-capacity hydrogen storage in lithium and sodium amidoboranes, Nat. Mater., 7 (2008) 138–41.

[32] G.R. Eaton, NMR of boron compounds, J. Chem. Educ., 46 (1969) 547–556.

[33] M.R. Hansen, T. Vosegaard, H.J. Jakobsen, J. Skibsted, ^{11}B chemical shift anisotropies in borates from ^{11}B MAS, MQMAS, and single-crystal NMR spectroscopy, J. Phys. Chem. A, 108 (2004) 586–594.

[34] S. Hermanek, ^{11}B NMR Spectra of boranes, main-group heteroboranes, and substituted derivatives Factors influencing chemical shifts of skeletal atoms, Chem. Rev., 92 (1992) 325–362.

[35] V. Rizzi, D. Polino, E. Sicilia, N. Russo, M. Parrinello, The onset of dehydrogenation in solid ammonia borane: An ab initio metadynamics study, Angew. Chemie, 131 (2019) 4016–4020.

[36] A.C. Stowe, W.J. Shaw, J.C. Linehan, B. Schmid, T. Autrey, In situ solid state ^{11}B MAS-NMR studies of the thermal decomposition of ammonia borane: Mechanistic studies of the hydrogen release pathways from a solid state hydrogen storage material, Phys. Chem. Chem. Phys., 9 (2007) 1831–1836.

[37] T. Kobayashi, S. Gupta, M.A. Caporini, V.K. Pecharsky, M. Pruski, Mechanism of solid-state thermolysis of ammonia borane: A ^{15}N NMR study using fast magic-angle spinning and dynamic nuclear polarization, J. Phys. Chem. C, 118 (2014) 19548–19555.

[38] T. Chatterjee, S.T. Thynell, Development of a reaction mechanism for liquid-phase decomposition of ammonia borane, Thermochim. Acta, 682 (2019) 178427.

[39] X. Chen, X. Bao, J.C. Zhao, S.G. Shore, Experimental and computational study of the formation mechanism of the diammoniate of diborane: The role of dihydrogen bonds, J. Am. Chem. Soc., 133 (2011) 14172–14175.

[40] T. Banu, K. Sen, T. Ash, A.K. Das, Dehydrogenation of lithium hydrazinidoborane: Insight from computational analysis, Int. J. Hydrog. Energy, 41 (2016) 18953–18962.

[41] T. Li, K. Wang, J.G. Zhang, Theoretical study of the structure and dehydrogenation mechanism of sodium hydrazinidoborane, J. Theor. Comput. Chem., 16 (2017) 1–13.

[42] S.A. Shevlin, B. Kerkeni, Z.X. Guo, Dehydrogenation mechanisms and thermodynamics of MNH_2BH_3 (M = Li, Na) metal amidoboranes as predicted from first principles, Phys. Chem. Chem. Phys., 13 (2011) 7649–7659.

[43] L. Li, Q. Gu, Z. Tang, X. Chen, Y. Tan, Q. Li, X. Yu, Two novel derivatives of ammonia borane for hydrogen storage: Synthesis, structure, and hydrogen desorption investigation, J. Mater. Chem. A, 1 (2013) 12263–12269.

[44] D.P. Kim, K.T. Moon, J.G. Kho, J. Economy, C. Gervais, F. Babonneau, Synthesis and characterization of poly-(aminoborane) as a new boron nitride precursor, Polym. Adv. Technol., 10 (1999) 702–712.

[45] C. Gervais, E. Framery, C. Duriez, J. Maquet, M. Vaultier, F. Babonneau, ^{11}B and ^{15}N solid state NMR investigation of a boron nitride preceramic polymer prepared by ammonolysis of borazine, J. Eur. Ceram. Soc., 25 (2005) 129–135.

[46] C. Gervais, J. Maquet, F. Babonneau, C. Duriez, E. Framery, M. Vaultier, P. Florian, D. Massiot, Chemically derived BN ceramics: Extensive ^{11}B and ^{15}N solid-state NMR study of a preceramic polyborazilene, Chem. Mater., 13 (2001) 1700–1707.

[47] B. Roy, U. Pal, A. Bishnoi, L.A. O'Dell, P. Sharma, Exploring the homopolar dehydrocoupling of ammonia borane by solid-state multinuclear NMR spectroscopy, Chem. Commun., (2021) 1887–1890.

[48] S.K. Sahoo, J.P. Dhal, G.K. Panigrahi, Magnesium oxide nanoparticles decorated iron oxide nanorods: Synthesis, characterization and remediation of Congo red dye from aqueous media, Compos. Commun., 22 (2020) 100496.

[49] I. Karuppusamy, M.S. Samuel, E. Selvarajan, S. Shanmugam, P. Sahaya Murphin Kumar, K. Brindhadevi, A. Pugazhendhi, Ultrasound-assisted synthesis of mixed calcium magnesium oxide ($CaMgO_2$) nanoflakes for photocatalytic degradation of methylene blue, J. Colloid Interface Sci., 584 (2021) 770–778.

[50] K. Vijai Anand, A.R. Anugraga, M. Kannan, G. Singaravelu, K. Govindaraju, Bio-

engineered magnesium oxide nanoparticles as nano-priming agent for enhancing seed germination and seedling vigour of green gram (Vigna radiata L), Mater. Lett., 271 (2020) 127792.

[51] A. Kondo, R. Kurosawa, J. Ryu, M. Matsuoka, M. Takeuchi, Investigation on the mechanisms of $Mg(OH)_2$ dehydration and MgO hydration by near-infrared spectroscopy, J. Phys. Chem. C, 125 (2021) 10937–10947.

[52] W. Lei, D. Liu, Y. Chen, Highly crumpled boron nitride nanosheets as adsorbents: Scalable solvent-less production, Adv. Mater. Interfaces, 2 (2015) 2–7.

[53] J.I. Oñate, A. García, V. Bellido, J.L. Viviente, Deposition of hydrogenated B-C thin films and their mechanical and chemical characterization, Surf. Coatings Technol., 49 (1991) 548–553.

[54] D. Schild, S. Ulrich, J. Ye, M. Stüber, XPS investigations of thick, oxygen-containing cubic boron nitride coatings, Solid State Sci., 12 (2010) 1903–1906.

[55] D.M. Marincel, M. Adnan, J. Ma, E.A. Bengio, M.A. Trafford, O. Kleinerman, D. V. Kosynkin, S.H. Chu, C. Park, S.J.A. Hocker, C.C. Fay, S. Arepalli, A.A. Martí, Y. Talmon, M. Pasquali, Scalable purification of boron nitride nanotubes via wetthermal etching, Chem. Mater., 31 (2019) 1520–1527.

[56] N. Badi, High temperature dielectric properties of ($B_xN_yO_z$) thin films deposited using ion source assisted physical vapor deposition, J. Adv. Dielectr., 5 (2015).

[57] D.J. Alberas, J. Kiss, Z.M. Liu, J.M. White, Surface chemistry of hydrazine on Pt(111), Surf. Sci., 278 (1992) 51–61.

[58] P. Bachmann, F. Düll, F. Späth, U. Bauer, H.P. Steinrück, C. Papp, A HR-XPS study of the formation of h-BN on Ni(111) from the two precursors, ammonia borane and borazine, J. Chem. Phys., 149 (2018).

[59] J.C. Fuggle, L.M. Watson, D.J. Fabian, S. Affrossman, X-ray excited Auger and photoelectron spectra of magnesium, some alloys of magnesium and its oxide, J. Phys. F Met. Phys., 5 (1975) 375–383.

[60] L. Crociani, G. Rossetto, S. Kaciulis, A. Mezzi, N. El-Habra, V. Palmieri, Study of magnesium boride films obtained from $Mg(BH_4)_2$ by CVD, Chem. Vap. Depos., 13 (2007) 414–419.

[61] L. Crociani, G. Carta, S. Kaciulis, A. Mezzi, G. Rossetto, P. Zanella, Chemical composition of magnesium boride films obtained by CVD, Surf. Interface Anal., 40 (2008) 741–745.

[62] U. Gulati, U. Chinna Rajesh, D.S. Rawat, J.M. Zaleski, Development of magnesium oxide-silver hybrid nanocatalysts for synergistic carbon dioxide activation to afford esters and heterocycles at ambient pressure, Green Chem., 22 (2020) 3170–3177.

[63] D.J. Wolstenholme, K.T. Traboulsee, Y. Hua, L.A. Calhoun, G.S. McGrady, Thermal desorption of hydrogen from ammonia borane: Unexpected role of homopolar B-H···H-B interactions, Chem. Commun., 48 (2012) 2597–2599.

[64] Y. Nakagawa, S. Isobe, Y. Ikarashi, S. Ohnuki, AB-MH (Ammonia Borane-Metal Hydride) composites: Systematic understanding of dehydrogenation properties, J. Mater. Chem. A, 2 (2014) 3926–3931.

[65] X. Kang, L. Ma, Z. Fang, L. Gao, J. Luo, S. Wang, P. Wang, Promoted hydrogen release from ammonia borane by mechanically milling with magnesium hydride: A new destabilizing approach, Phys. Chem. Chem. Phys., 11 (2009) 2507–2513.

[66] J. Luo, X. Kang, P. Wang, Synthesis, formation mechanism, and dehydrogenation properties of the long-sought $Mg(NH_2BH_3)_2$ compound, Energy Environ. Sci., 6 (2013) 1018–1025.

[67] A.T. Luedtke, T. Autrey, Hydrogen release studies of alkali metal amidoboranes, Inorg. Chem., 49 (2010) 3905–3910.

[68] S. Frueh, R. Kellett, C. Mallery, T. Molter, W.S. Willis, C. King'Ondu, S.L. Suib, Pyrolytic decomposition of ammonia borane to boron nitride, Inorg. Chem., 50 (2011) 783–792.

[69] G.B. Manelis, V. V. Zakharov, G.N. Nechiporenko, V.A. Strunin, A. V. Raevskii, V. V. Yakovlev, Combustion and thermal decomposition of hydrazine borane, Combust. Explos.

Shock Waves, 51 (2015) 462–466.

[70] M. Noura, A. Rahdar, S.M. Taimoory, J.J. Hayward, S.I. Sadraei, J.F. Trant, A theoretical first principles computational investigation into the potential of aluminum-doped boron nitride nanotubes for hydrogen storage, Int. J. Hydrog. Energy, 45 (2020) 11176–11189.

[71] L. Ma, L. Wang, Y. Sun, L. Ma, J. Zhang, First-principles study of hydrogen storage on Ca-decorated defective boron nitride nanosheets, Phys. E Low-Dimensional Syst. Nanostructures, 128 (2021) 114588.

[72] A. Hajari, B. Roy, P. Sharma, Metal-free rapid dehydrogenation kinetics and better regeneration yield of ammonia borane (in press), Int. J. Hydrog. Energy, XX (2021) XX–XX.

[73] Z. Tang, L. Zhang, L. Wan, Z. Huang, H. Liu, Z. Guo, X. Yu, Regeneration of alkaline metal amidoboranes with high purity, Int. J. Hydrog. Energy, 41 (2016) 407–412.

[74] Y. Tan, L. Zhang, X. Chen, X. Yu, Reductive dechlorination of BCl_3 for efficient ammonia borane regeneration, Dalt. Trans., 44 (2015) 753–757.

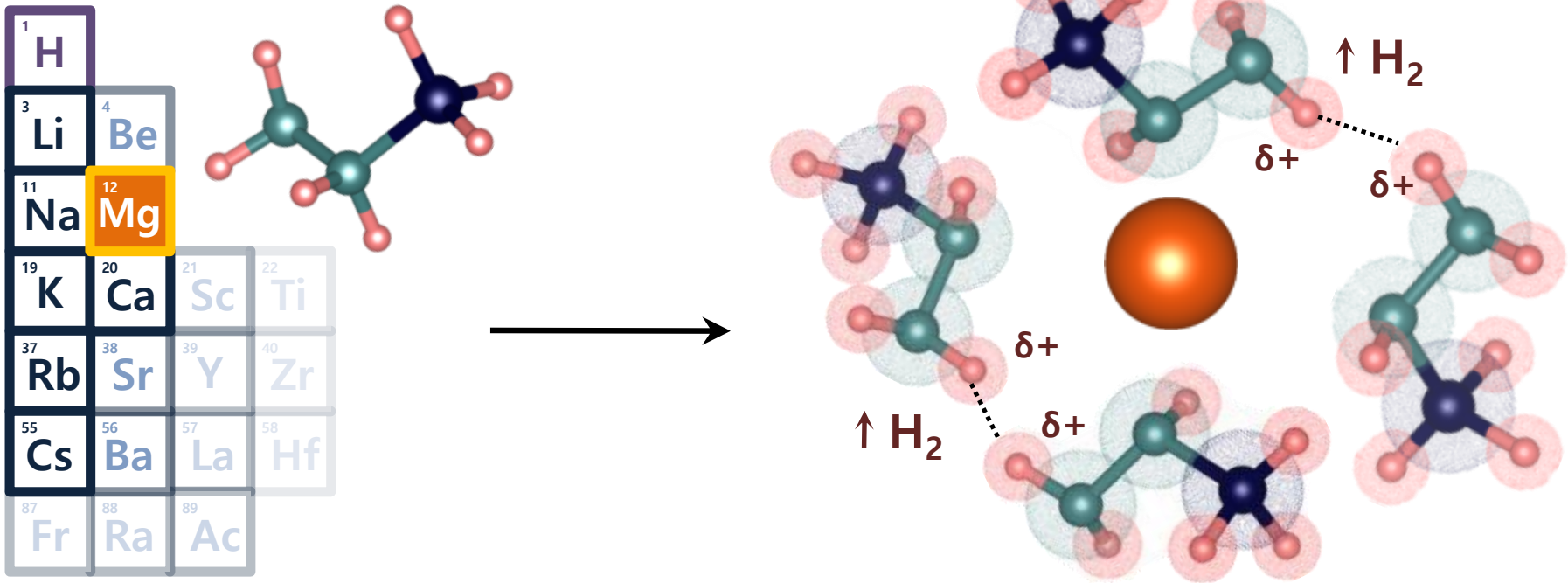
1 H
3 Li
4 Be
11 Na
12 Mg
19 K
20 Ca
21 Sc
22 Ti
37 Rb
38 Sr
39 Y
40 Zr
55 Cs
56 Ba
57 La
58 Hf
87 Fr
88 Ra
89 Ac
↑ H2
δ+
δ+
δ+
↑ H2
δ+